scientific reports

Check for updates

OPEN

Spatial transcriptomic map of the mouse urinary bladder

Nives Matković[1], Andrea Gelemanović[2], Kristijana Popović[1], Katarina Vilović[1,3], Caterina Oneto[4], Dejan Lazarević[4], Ivana Marinović Terzić[1], Ivana Novak[1], Jelena Korac-Prlic[1], Blanka Milić Roje[5] & Janoš Terzić[1]✉

We present a spatial transcriptomic map of the mouse urinary bladder at near single-cell resolution using Visium HD technology with 8 × 8 µm bins. After quality filtering, we analyzed 66,471 bins and 9,364 genes. Cluster annotation was supported by canonical marker genes and reference datasets, including Tabula Muris and Mouse Cell Atlas. Thirteen distinct clusters corresponding to major bladder compartments—the urothelium, lamina propria, and smooth muscle—were identified. Gene expression patterns revealed gradual transitions across tissue layers rather than sharp boundaries. Within the urothelium, basal, intermediate, and umbrella cells were distinguished, with umbrella cells showing potentially polarized mRNA distribution. The lamina propria primarily consisted of fibroblasts and a small number of immune cells. Four smooth muscle clusters were detected, contrasting with the single cluster typically identified by non-spatial single-cell RNA sequencing. This spatially resolved transcriptome map highlights the advantages of spatial transcriptomics in complementing traditional histology and scRNA-seq. Our map provides a valuable resource for advancing understanding of mouse urinary bladder biology and establishes a foundation for future studies of bladder pathology.

Keywords mouse urinary bladder, spatial transcriptomics, urothelium, lamina propria, smooth muscle

This study aims to generate a comprehensive spatial transcriptomic (ST) map of the mouse urinary bladder. While not focused on bladder cancer, we chose the bladder as our primary organ of interest due to its relevance—bladder cancer ranks among the ten most common cancers globally[1]. Establishing a healthy spatial transcriptomic baseline is essential for advancing future diagnostics.

A major strength of our approach is the use of high-resolution ST technology, detecting mRNA in 8 × 8 µm bins. This bin size offers a balance between spatial resolution and transcript capture, approximating the size of the smallest bladder cells (e.g., basal and intermediate urothelial cells)[2], enabling near single-cell resolution. Larger cells like umbrella cells[2] span multiple bins, allowing assessment of their spatial heterogeneity. While higher resolutions (e.g., 2 × 2 µm) are possible, they often yield fewer transcripts per bin, compromising data quality. Conversely, larger bins (10 × 10 or 12 × 12 µm) reduce spatial precision. Thus, 8 × 8 µm represents an optimal trade-off, capturing diverse cell types while maintaining a strong spatial and molecular signal.

The techniques and analysis pipelines used here are applicable to other tissues and organs. Given the difficulty of obtaining truly healthy control tissues, our data provide a valuable molecular reference. These findings can also enhance understanding of cell-to-cell communication across bladder tissue layers.

Histologically, bladder tissue comprises the urothelium, lamina propria, tunica muscularis, and outer tunica serosa/adventitia[3]. Spatial transcriptomics adds molecular depth to this classification[4]. Known tissue-specific genes serve as a framework to interpret ST data. Literature identifies several markers characteristic of specific layers — e.g., uroplakins and cytokeratin CK20 mark umbrella cells[5]. To our knowledge, this is the first study to characterize spatially distinct cell clusters in the mouse urinary bladder based on established gene expression markers.

Urinary epithelium

The epithelium is the innermost layer lining hollow organs, serving as the first line of defense and structural barrier[2]. In the urinary bladder, this layer—called the urothelium—is a specialized, stratified transitional epithelium adapted to withstand the mechanical and chemical stress from urine[6]. As a filtrate of blood, urine

[1]Laboratory for Cancer Research, School of Medicine, University of Split, Split, Croatia. [2]Mediterranean Institute for Life Sciences, University of Split, Split, Croatia. [3]Department of Pathology, University Hospital of Split, Split, Croatia. [4]Center for Translational Genomics and Bioinformatics, San Raffaele Scientific Institute, Milan, Italy. [5]Institute of Oceanography and Fisheries, Split, Croatia. ✉email: janos.terzic@mefst.hr

contains excess metabolic products and can vary in pH, creating acidic or alkaline environments in which epithelial cells reside until voiding[3,7]. To maintain impermeability, urothelial cells form tight junctions that prevent urine penetration into deeper tissue layers. Meanwhile, the bladder must distend to accommodate varying volumes of urine, a function supported by both the underlying detrusor muscle and the extensibility of the urothelium itself[6,8].

The urothelium comprises three distinct cell types: umbrella, intermediate, and basal cells[2].

Umbrella cells, forming the outermost layer, are specialized for bladder expansion. Dome-shaped and often binuclear, they can range from 25 to 250 µm in length and are significantly larger and octoploid compared to other urothelial cells[3,8]. These cells feature both tight and adherent junctions and are marked by uroplakins (*Upk*) and cytokeratin 20 (*CK20* in humans, *Krt20* in mice). Umbrella cells in both species express *Upk1a*, *Upk1b*, *Upk2*, and *Upk3a*, which assemble into asymmetric unit membrane (AUM) structures. Although their function is not fully understood[6], uroplakin-deficient mice exhibit structurally compromised umbrella cells[3]. Notably, *Upk1a* serves as a receptor for uropathogenic *E. coli*[6,9], a major contributor to bladder inflammation. Given the link between chronic inflammation and cancer risk[10], uroplakins may play a key protective role.

Intermediate cells lie beneath umbrella cells and vary in layering depending on species—multiple layers in humans, typically a monolayer in mice[6,11]. Around 20 µm in size, these cells are interconnected by desmosomes and express uroplakin 2, claudin, and e-cadherin, though their tight junctions are less prominent than in umbrella cells[6]. p63 and sonic hedgehog (*Shh*) are also expressed but are not unique to this layer[2].

Basal cells form the deepest layer, attaching to the basement membrane via hemidesmosomes. Measuring 5–10 µm, they are the smallest and most numerous urothelial cells, likely containing stem cells responsible for regeneration. Basal cells express *CK5*, *p63*, and *Shh*, but not *CK20* or uroplakins, distinguishing them from the upper layers[2].

The lamina propria

The lamina propria is a connective tissue region between the urothelium's basement membrane and the detrusor muscle[12]. It forms the organ's stroma, containing fibroblasts, vascular smooth muscle cells, and immune cells that support structural integrity, vascularization, and immune function. It also acts as a capacitance layer, adjusting to bladder volume[12].

Fibroblasts

Fibroblasts are the main cell type in the bladder lamina propria, producing extracellular matrix components to maintain tissue structure. *Pdgfra*$^+$ is a widely accepted marker for identifying fibroblasts, though it does not label all fibroblast subtypes[13–15].

Suburothelial Fibroblasts

Located just beneath basal urothelial cells, suburothelial fibroblasts are *Tnc*$^+$ *Cd34*$^-$ and express *Acta2*, *Ptgs1*, *Bmp5*, *Bmp7*, and *Cxcl14*[13]. Using single-cell sequencing and Acta2-GFP reporter mice, their location was confirmed. Baker et al.. identified these cells via *Car3* and *Cxcl14* markers using imaging mass cytometry[16], and Visium v2 ST (55 µm resolution) confirmed *Car3*$^+$ localization. Gene expression and ultrastructural studies revealed four fibroblast subgroups, two of which are in the lamina propria[14]. Suburothelial fibroblasts are enriched for *Acta2*, *Car3*, *Ly6A*, *Myg10*, *Tnc*, *Vim*, *Col1a2*, and *Col15a1*.

There is ongoing debate over whether *Acta2*$^+$ suburothelial cells are fibroblasts or myofibroblasts[13,14,17]. Some evidence suggests myofibroblasts arise from fibroblasts after tissue damage[14,18]. While typical myofibroblast ultrastructures (e.g., fibronexus) are absent[14,15], the role of this structure as a definitive marker is unclear. Its presence may reflect a functional rather than a structural state. These uncertainties highlight the need for better-defined fibroblast and myofibroblast markers.

Outer lamina propria fibroblasts

Located deeper in the lamina propria, *Tnc*$^-$/*Cd34*$^+$ fibroblasts are distinguished from suburothelial fibroblasts[13]. Baker et al.. marked this population using *Npy1r*, though cross-species homology remains unclear[16]. Clayton et al.. define them by *Cd34*, *Ly6A*, *Pi16*, *Vim*, *Col1a2*, and *Col15a1*[14].

Buechler et al.. identified two universal fibroblast subtypes across murine tissues based on *Col15a1* and *Pi16* expression[19]. Clayton et al.. showed that suburothelial fibroblasts express *Col15a1* but not *Pi16*, whereas outer lamina propria fibroblasts express both, indicating spatial and functional distinctions.

The urinary bladder immune cells

Immune cells in the urinary bladder mainly reside in the lamina propria and muscle tissue. Although present in small numbers, they are primed for rapid immune responses involving recruitment of circulating cells, which differ in origin from tissue-resident immune cells. Cd45 is a general immune cell marker, but specific cell types require distinct markers. About 70% of bladder immune cells are antigen-presenting cells, primarily macrophages (F4/80^{hi} Ly6C$^-$) and dendritic cells (Cd11b$^+$, Cd8α/Cd103$^+$). Other immune cells include ILCs (Cd25$^+$, Cd127$^+$), NK cells (Cd49a$^+$), and T cells (Cd4$^+$, Cd8$^+$)[20].

The urinary bladder smooth muscle

The *tunica muscularis* of the urinary bladder forms its thick muscular wall. Smooth muscle cells (myocytes) are spindle-shaped and shorter than skeletal muscle fibers, measuring 20 to 500 µm in length[7,21,22]. The tunica muscularis is divided into three histologically distinct regions: the detrusor, trigone, and ureteral muscles. The detrusor muscle comprises the largest area, made up of smooth muscle cells arranged in loosely defined longitudinal, circular, and oblique bundles organized into three layers[23]. These fibers are enveloped by a basement

membrane connected to a loose collagen network, forming the connective tissue known as the endomysium. The detrusor's elasticity allows it to stretch during filling and contract fully to expel urine[7].

Jaslove and Nelson reviewed smooth muscle's role in epithelial formation and listed the 25 most expressed genes, including canonical markers *Acta2*, *Actg2* (γ-smooth muscle actin), *Myh11*, transgelin (*Tagln*), calponin (*Cnn*), and caldesmon (*Cald1*)[21]. Han et al.. provided a single-cell transcriptomic map of the mouse bladder, listing 347 smooth muscle genes, with top markers including *Acta2*, *Myl9*, *Tagln*, *Myh11*, *Cnn*, and *Tpm2*[24]. Common markers in both studies are *Acta2*, *Tagln*, and *Cnn*[21,24].

In an unpublished preprint, Baker et al.. reported low-resolution spatial transcriptomics of the mouse bladder, identifying three clusters: one corresponding to the detrusor, one to pericytes (*Rgs5*, *Kcnj8*, *Pdgfrb*), and one to vascular smooth muscle cells (*vSMC*; *Tesc*, *Pln*, *Wtip*)[16]. All clusters expressed general smooth muscle markers *Acta2*, *Myl9*, *Mylk*, while the detrusor cluster was specifically marked by *Actg2*, *Acta1*, and *Tnnt2*[16]. Despite histological and transcriptomic divisions into three categories, these classifications do not completely overlap[7,16].

The summary of all the marker genes for different tissue layers of the urinary bladder found in the literature to date is shown in Table 1.

Results

Complete ST (spatial transcriptomics) dataset of healthy murine bladder consisted of 19,059 genes across 165,781 bins (8 × 8 µm, approximating single-cell resolution). After quality control filtering for low transcript counts and high mitochondrial gene content, 66,471 bins remained for downstream bioinformatics analysis following the standard R package Seurat[25] workflow for spatial transcriptomics. The Seurat pipeline provided dimensionality reduction, cluster identification, and differential gene expression.

Upon the SCTransform method for normalization, which considers the high-dimensionality and sparsity of single-cell data, the dataset was reduced to 9,364 genes, including 3,000 highly variable genes. First to reduce the noise, principal component analysis (PCA) dimensionality reduction was performed which retained the first 8 principal components for downstream analysis as the most significant sources of variation within the data. Finally, to identify clusters and visualize them into two dimensions, UMAP (Uniform Manifold Approximation and Projection) was performed, and 13 distinct clusters were identified at resolution of 0.6[26].

Unsupervised clustering and spatial mapping of transcriptomic signatures in bladder tissue

Cluster-specific marker genes were identified using the Seurat function FindAllMarkers. A complete list of differentially expressed gene markers for each cluster is provided in Supplementary Table S1. Top marker genes are highlighted in yellow and are defined as genes expressed in at least 40% of bins (approximately resembling cells) with a $\log_2$ fold change of at least 0.25. Additionally, Supplementary Table S2 lists up to the tenth most-expressed genes for each cluster. Cluster annotation was confirmed by reference data from Tabula Muris[27], Mouse Cell Atlas[24], as well as markers listed in the literature review in the introduction of this paper[2,3,6,7,12,14,16]. Throughout, spatial localization was achieved by overlaying spatial barcode coordinates with histological stratification.

The comprehensive workflow of the experimental and computational pipelines from formalin-fixes paraffin embedded (FFPE) tissue sectioning through RNA sequencing and bioinformatic clustering using the Seurat package is shown in Fig. 1a. The hematoxylin-eosin (H&E) brightfield image (Fig. 1b) shows bladder histology with urothelium, lamina propria, and muscle layer.

Unsupervised clustering of obtained spatial transcripts reveals 13 distinct clusters (Fig. 1c) corresponding to major tissue compartments. Clusters are validated by canonical marker gene expression patterns summarized in the heatmap (Fig. 1d). Clusters annotated as urothelial clusters possessed expression of cytokeratin and uroplakin genes indicative of basal, intermediate, and umbrella cells. The smooth muscle clusters expressed canonical markers (*Tagln*, *Myh11*, *Acta2*) but varied in additional differentially expressed genes as shown in Supplementary Table S3. S3 presents a pairwise comparison of clusters within the same tissue layer, listing all genes differentially expressed between layer-specific clusters, e.g. smooth muscle A cluster versus smooth muscle B. Lamina propria clusters show collagen-related genes (*Col1a1*) characteristic of fibroblasts. Immune cells are located mostly in the lamina propria, although their presence is generally sparse. We found only 225 positive

Bladder tissue layer	Cell type	Markers
Urothelium [2]	Umbrella cells	*Krt20*, *Upk1a*, *Upk1b*, *Upk2*, *Upk3a*
	Intermediate cells	*Trp63*, *Shh*, *Upk2*
	Basal cells	*Krt5*, *Trp63*, *Shh*
Lamina propria [13–15]	suF	*Pdgfra*, *Tnc*, *Acta2*, *Ptgs1*, *Bmp5*, *Bmp7*, *Cxcl4*, *Car3*, *Col4a1*, *Col4a2*, *Ly6A*, *Myg10*, *Vim*, *Col15a1*
	olpF	*Pdgfra*, *Vim*, *Cd34*, *Ly6A*, *Pi16*, *Col1a2*, *Col15a1*
Smooth muscle [16,21,24]	General	*Acta2*, *Myl9*, *Tagln*, *Myh11*, *Cnn1*, *Tpm2*
	m. detrusor	*Actg2*, *Tnnt2*, *Acta1*
	vSMC	*Tesc*, *Pln*, *Wtip*
	Pericytes	*Rgs5*, *Kcnj8*, *Pdgfrb*

Table 1. The summary of bladder tissue layer markers from the literature review. *suF* suburothelial fibroblasts, *olpF* outer lamina propria fibroblasts; vSMC – vascular smooth muscle cells.

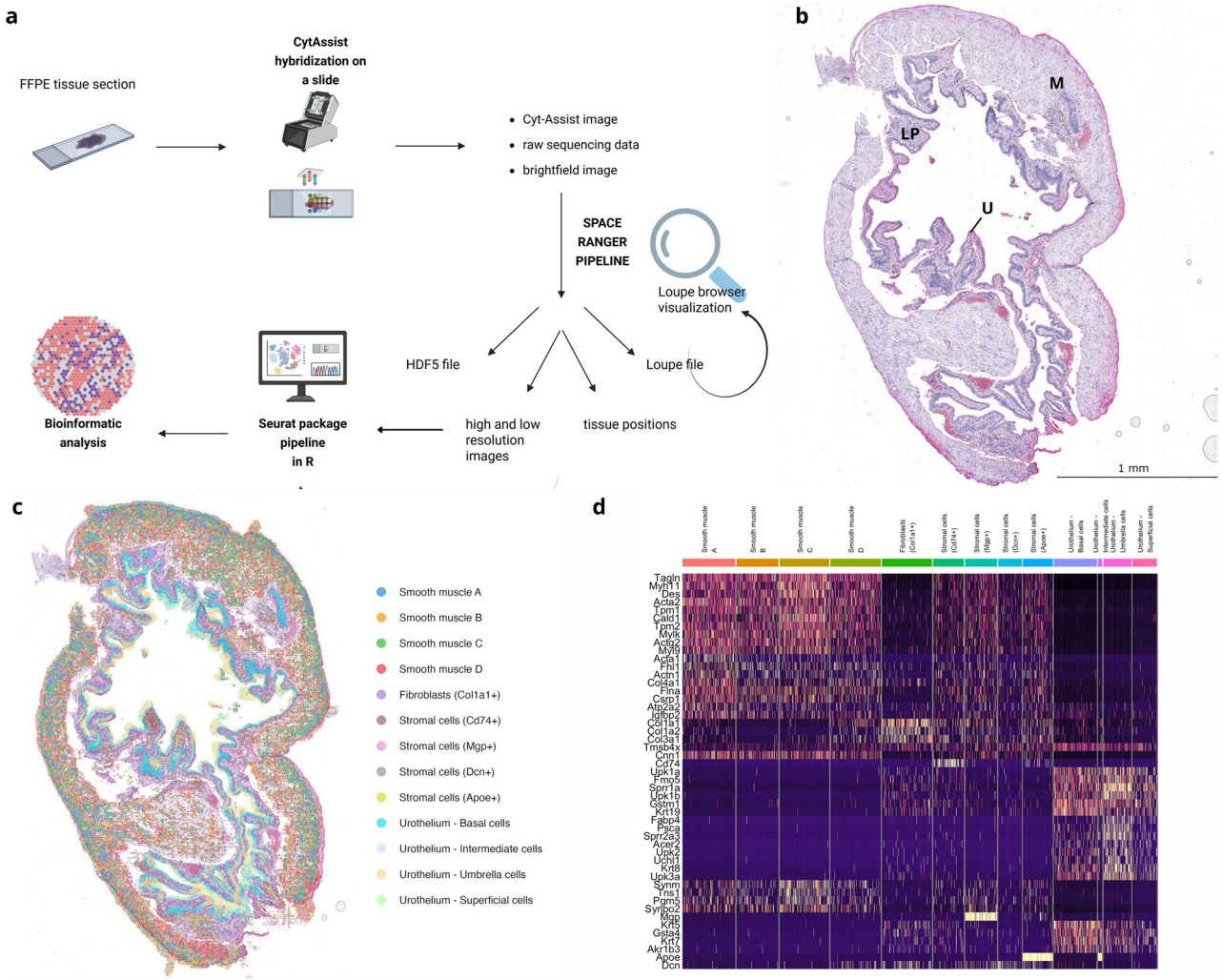

Fig. 1. Integrated workflow and spatial transcriptomic profiling of mouse bladder tissue. (**a**) Schematic overview of the experimental and bioinformatic workflow, from FFPE tissue sectioning to spatial transcriptomic analysis using the Seurat package in R. Figure created with BioRender.com. (**b**) Representative H&E-stained brightfield image of whole bladder tissue section, highlighting histologic features. U – urothelium. LP – lamina propria. M – muscle. (**c**) Spatial mapping of transcriptomic clusters across the bladder tissue, showing distinctive cell types and anatomical regions identified by the Seurat pipeline. (**d**) Heatmap summarizing up to the top 10 differentially expressed (DE) marker genes (Features) per each spatial cluster (Identity) according to the set thresholds (see Methods section) with colour representing percentage of cells expressing each gene and average expression level, respectively. The top differentially expressed gene for stromal clusters are indicated in parentheses adjacent to the cluster name.

bins for *Cd45* (*Ptprc*), with 30 *Cd4* positive bins and 24 *Cd8* positive bins. The most abundant immune-related cell type present in 3808 bins was antigen-presenting cells marked with *Cd74* (Fig. 2).

Further analysis (Fig. 2) visualizes global transcriptional activity across the tissue using Seurat-generated spatial feature plots. Overall, the highest expression activity is observed in the urothelial layer (Fig. 2a). Yellow zones indicate high gene expression, which corresponds to the urothelium. The UMAP plot of clusters (Fig. 2b) emphasizes the transcriptomic diversity and relatedness of the identified cell populations. Spatial localization of top genes per cluster is shown in Fig. 2c. Figure 2d shows two-dimensional UMAP plots of the top gene expression patterns, which correspond to the 13 clusters identified in Fig. 2b. Although some clusters share the same top gene, their distinct expression profiles and spatial distributions reflect underlying molecular heterogeneity and spatial gradients within the tissue.

Fine-scale spatial transcriptomics and clustering elucidates cellular heterogeneity in urothelium and smooth muscle

A defined bladder tissue region was examined in detail using Loupe Browser with imported Seurat-filtered datasets (Fig. 3).

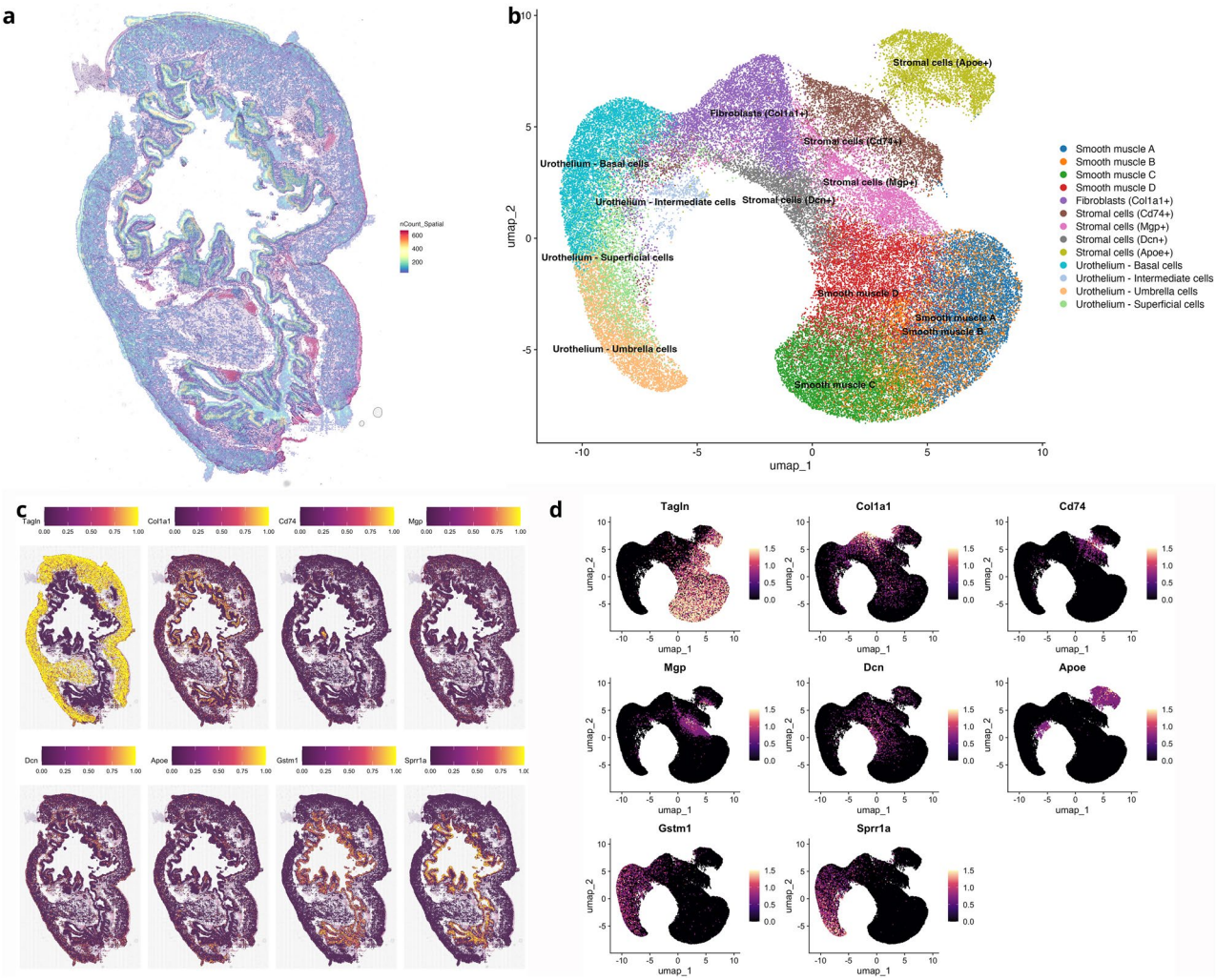

Fig. 2. High-resolution spatial and transcriptomic analysis of bladder tissue generated using the Seurat package in R. (**a**) Expression distribution map showing global transcriptional activity across the tissue section, with yellow indicating regions of higher gene expression and blue indicating lower activity. (**b**) UMAP plot depicting the two-dimensional representation of clusters obtained from the spatial transcriptomics dataset, highlighting the diversity and organization of cell populations within the sample. The top differentially expressed gene for stromal clusters are indicated in parentheses adjacent to the cluster name. (**c**) Spatial feature plots illustrating the localized expression of cluster-specific marker genes within the histological context of the tissue. (**d**) Feature plots presenting UMAP-reduced two-dimensional localization of top genes per cluster, visualizing molecular heterogeneity across the tissue.

The overview bladder tissue image (Fig. 3a) is accompanied by a magnified region of interest (Fig. 3b). Within this region, spatial maps show precise localization of urothelial markers such as *Krt20*, *Upk1a*, *Upk1b*, *Upk2*, *Upk3a*, and *Sprr1a* (Fig. 3c) and lamina propria markers including *Col1a1*, *Car3*, *Cd34*, and *Npy1r* (Fig. 3d). Smooth muscle markers *Tagln*, *Acta2*, *Actg2*, *Myh11*, *Myl9*, *Tpm1*, *Tpm2*, *Cnn1*, *Cald1*, and *Des* are represented in Fig. 3e. Alongside confirmation of proper transcript localization of key markers found in literature (Table 1), this spatial representation shows an interesting bin gradient of the smooth muscle clusters; the highest number of bins is at the outer part of the smooth muscle layer slowly decreasing towards lamina propria (Fig. 3e). Clustering within this magnified section (Fig. 3f) reveals discrete transcriptomic populations consistent with histological architecture of the urinary bladder. The annotated clusters are spatially contextualized within the full tissue overview (Fig. 3g).

Out of four urothelial clusters, two affirm the biological and histological stratification of the urothelium – basal and intermediate urothelial cells. By applying Seurat function AddModuleScore, which calculates the relative expression of a set of predefined marker genes, cluster 5 was shown to be the most similar to basal cells and cluster 9 to umbrella cells (Supplementary Table S4) according to the markers from the literature review shown in Table 1. Although recognized as a specific umbrella cell marker, *Krt20* was not listed in the top 10 genes of the cluster annotated as umbrella cells (Fig. 1d and Supplementary Table S2). Furthermore, since intermediate cells express both umbrella and basal cell markers and the top genes in cluster 12 correlate with

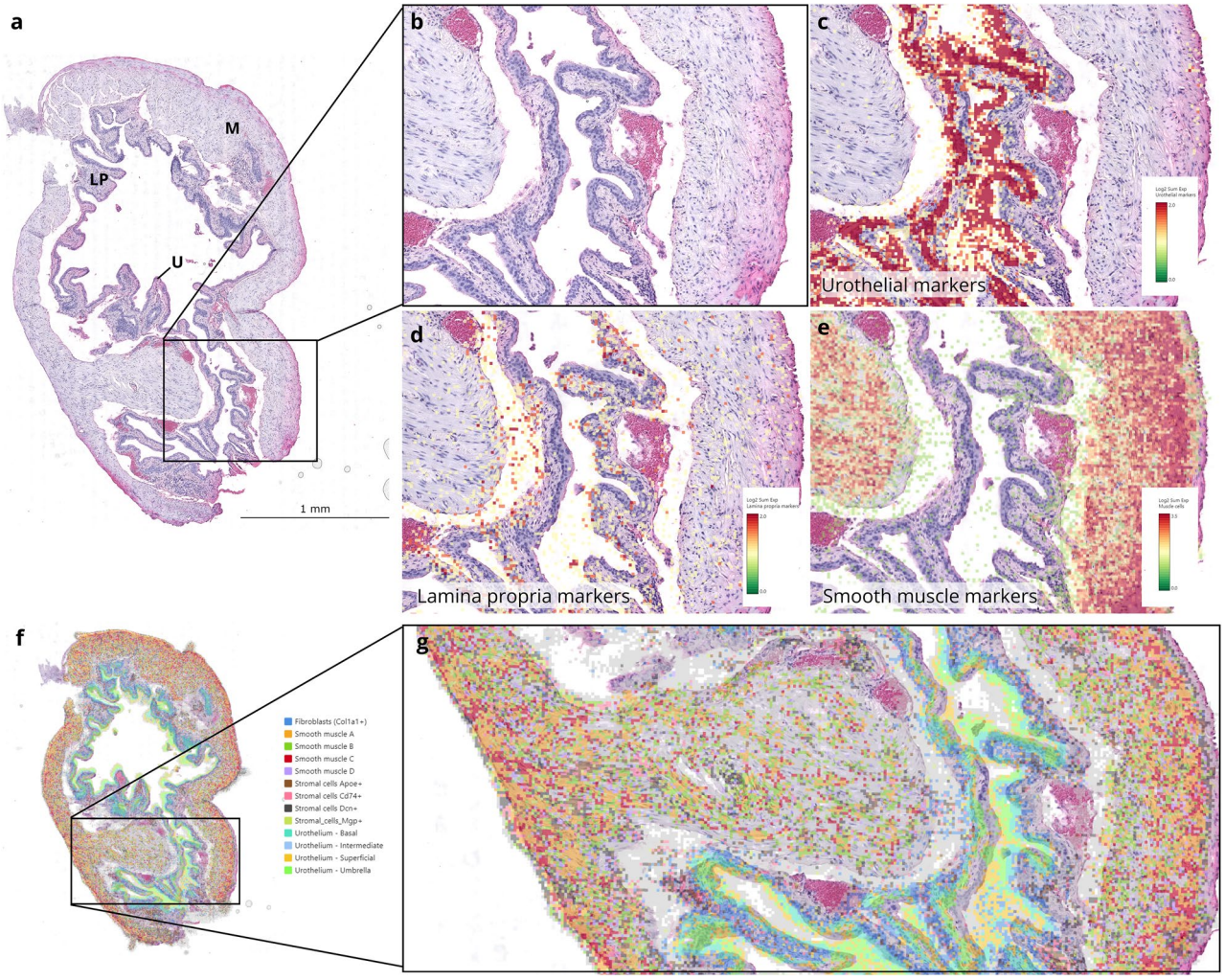

Fig. 3. Detailed spatial transcriptomic mapping of bladder tissue regions generated using Loupe Browser with integrated datasets filtered through the Seurat pipeline. (**a**) H&E-stained brightfield image of the entire bladder tissue section, highlighting the main layers: muscle (M), lamina propria (LP), and urothelium (U). (**b**) Magnified view of the selected region shown in panel A. (**c**) Magnified section displaying spatial expression of urothelial markers, including *Krt20*, *Upk1a*, *Upk1b*, *Upk2*, *Upk3a*, and *Sprr1a*. (**d**) Magnified section illustrating expression of lamina propria markers such as *Col1a1*, *Car3*, *Cd34* and *Npy1r*. (**e**) Magnified section showing smooth muscle markers including *Tagln*, *Acta2*, *Actg2*, *Myh11*, *Myl9*, *Tpm1*, *Tpm2*, *Cnn1*, *Cald1* and *Des*. (**f**) Clustered map of the magnified region highlighting distinct transcriptomic clusters representing different cell populations. (**g**) Overview image of the bladder tissue section with spatial transcriptomic clusters overlaid, corresponding to the region analyzed in panels (**b**) and (**f**). The top differentially expressed gene for each cluster is indicated in parentheses adjacent to the cluster name.

spatial localization, we assigned cluster 12 as an intermediate urothelial cell layer. One separate layer emerged above the layer annotated as umbrella cells. This layer showed reduced expression of several highly expressed genes in the umbrella cells cluster, such as *Psca*, *Fabp4*, *Upk2*, *Uchl1*, *Fam25c*, and *Tmem64* (S2 and S3). We annotated this cluster as superficial urothelium, noting that such a cluster has not been previously described. Figure 4 shows data stratification of the urothelial layers.

Our spatial transcriptomics analysis revealed distinct stromal cell populations within the bladder tissue, each characterized by unique marker expression and spatial localization. Fibroblasts (*Col1a1*$^{+}$) were broadly distributed throughout the lamina propria, while decorin-positive (*Dcn*$^{+}$) cells localized primarily toward the outer tissue layers. *Apoe*$^{+}$ cells clustered mainly within the lamina propria and immediate surroundings, and *Cd74*$^{+}$ stromal cells were present throughout the stromal compartment. *Mgp*$^{+}$ cells exhibited discrete, spatially restricted patterns. All these findings and their spatial organization are shown in Fig. 5, illustrating the heterogeneity and complex spatial arrangement of stromal cells in the bladder microenvironment.

In relation to the identified smooth muscle clusters, four clusters differentially express *Tagln*, *Tpm2*, *Myh11*, *Tpm1*, *Myl9*, *Mylk* and *Des* as their top 10 differentially expressed genes when compared to the whole transcriptome. Smooth muscle clusters are represented in Fig. 6.

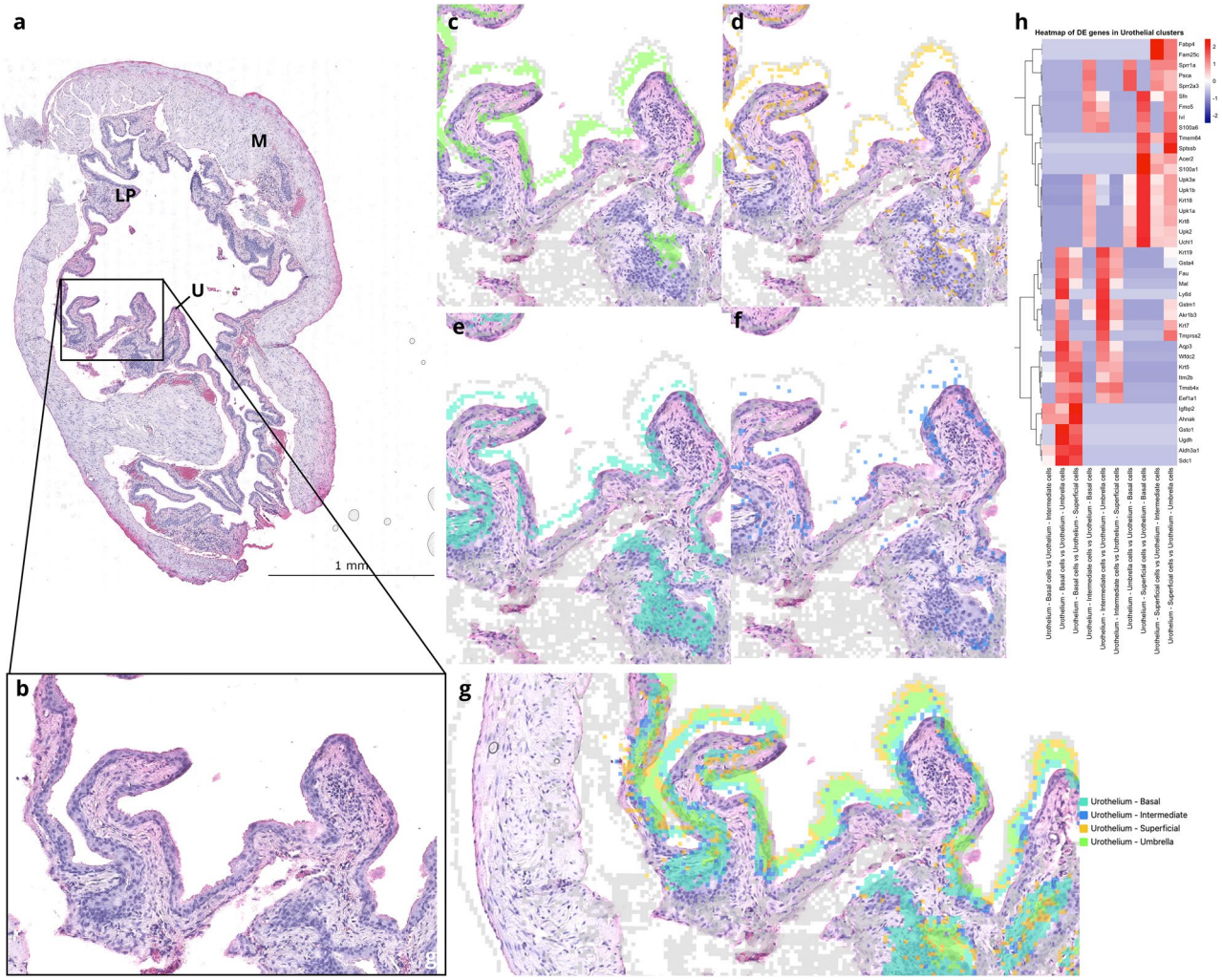

High-resolution spatial mapping and clustering of the bladder urothelial surface using integrated transcriptomic annotation in Loupe Browser. (**a**) H&E-stained brightfield image of the entire bladder tissue section, highlighting the main layers: M - muscle, LP - lamina propria, and U - urothelium. (**b**) Magnified view of the central urothelial region shown in panel a. (**c**) Spatial clustering displays a distinct umbrella cell population (green), traditionally described as the outermost urothelial layer in the literature. (**d**) Segmentation based on our dataset reveals an additional superficial urothelial layer (yellow) situated above the umbrella cells. (**e**) The basal urothelial cell layer is shown in cyan, representing the cell population resting on the basement membrane. (**f**) Spatial clustering reveals the intermediate urothelial cell layer (blue), positioned between the superficial layers and the basal layer. (**g**) Overlay visualization demonstrates the relative spatial organization of the superficial (yellow), umbrella (green), basal (cyan) and intermediate (blue) urothelial clusters, with the superficial cluster forming the outermost surface layer across the bladder epithelium in our data. Grey bins present in all layers represent low count areas filtered out by Seurat pipeline, but partially visible in Loupe. (**h**) Heatmap representing differentially expressed genes between the urothelial clusters (pairwise comparison).

We examined subtle differences among the smooth muscle clusters, all characterized by *Tagln* as their top differentially expressed gene, to elucidate the molecular basis underlying such clustering. Clusters were compared with each other to exclude common marker genes and identify significant differences. Smooth muscle A (Fig. 6c) cluster showed 4 positively correlated genes: *Flna*, *Csrp1*, *Fn1*, and *Igfbp2*. Even though all the smooth muscle clusters show differential expression of *Acta2* and *Actg2* in comparison to the whole dataset, Smooth muscle B (Fig. 6d) has shown the highest expression of those markers when compared to the other three smooth muscle clusters (S3). The Smooth muscle C cluster (Fig. 6e) is characterized by the distinct differential expression of *Synpo2* and *Synm*. This specificity is reflected in the top 10 differentially expressed genes listed in Supplementary Table S2 and is further supported by the pairwise comparisons among clusters shown in Supplementary Table S3. Smooth muscle D cluster (Fig. 6f) is the only cluster expressing collagen gene *Col1a1* alongside the key smooth muscle markers (S2 and S3).

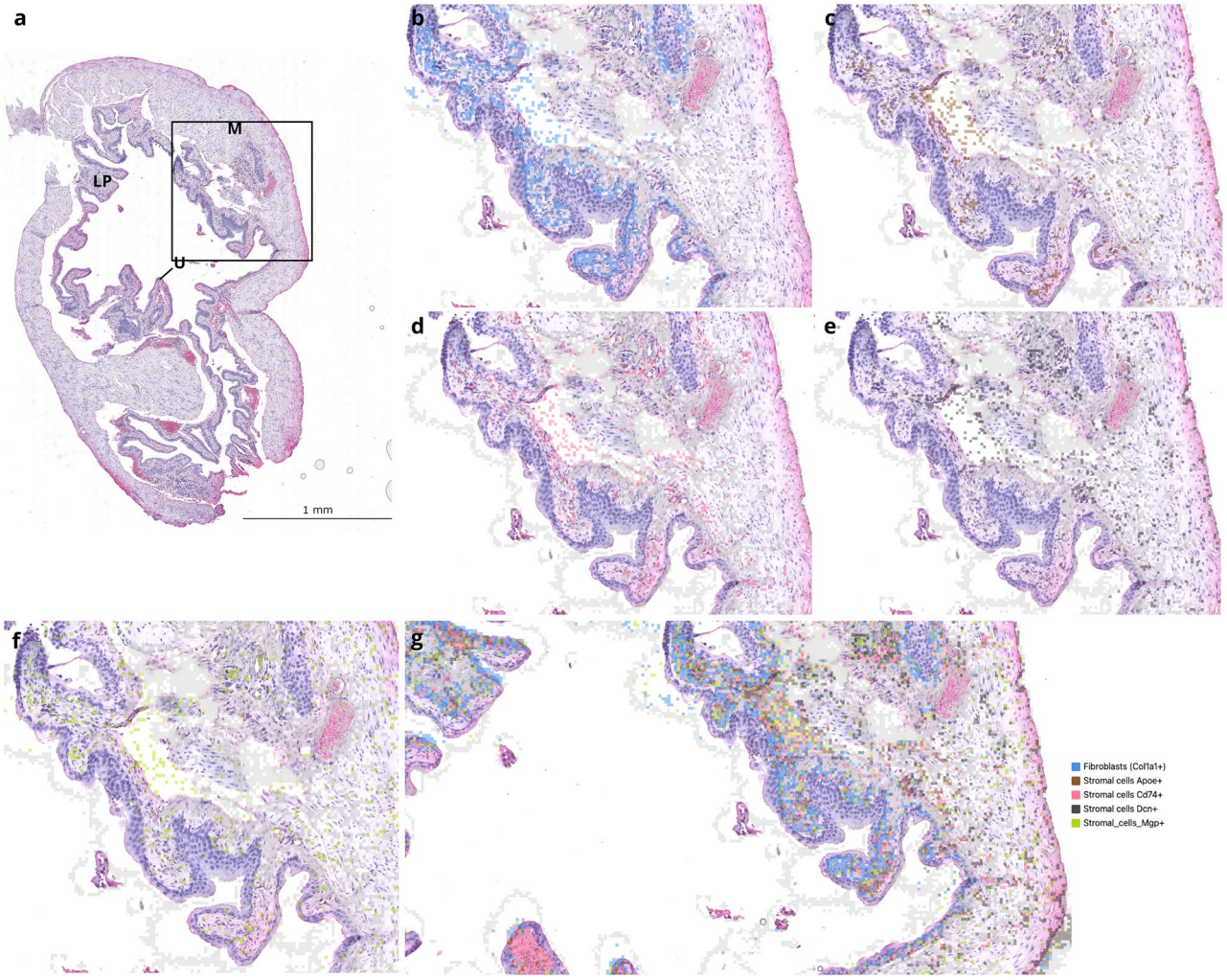

Fig. 5. High resolution spatial mapping and clustering of stromal cells populations in the bladder using integrated transcriptomic annotation in Loupe Browser. (**a**) H&E-stained brightfield image of the entire bladder tissue section, highlighting the main layers: M - muscle, LP - lamina propria, and U - urothelium. (**b**) Spatial clustering reveals the fibroblast population (*Col1a1*$^{+}$, blue), distributed throughout the lamina propria. (**c**) *Apoe*$^{+}$ stromal cells (brown) demonstrate specific clustering mostly within the lamina propria and in surrounding regions. (**d**) *Cd74*$^{+}$ stromal cells (pink) are visualized in their characteristic spatial context across the stromal compartment all over the tissue. (**e**) *Dcn*$^{+}$ stromal cells (decorin-positive, dark grey) show distinct localization patterns within the bladder stroma, localizing mostly towards the outer tissue layer. (**f**) *Mgp*$^{+}$ stromal cells (green) form discrete clusters highlighting unique spatial distribution in the bladder connective tissue. (**g**) Overlay visualization of all identified stromal cell populations (**b**–**f**) illustrates their relative spatial organization and relationships within the lamina propria and adjacent connective tissues.

Discussion

This is the first time a high-resolution, near-single-cell spatial transcriptomic map of the mouse urinary bladder has been created, providing unprecedented insight into gene expression patterns within intact tissue. This allows researchers to map gene expression to the exact location within tissue, providing a valuable resource that can be leveraged by others in the field to better understand cellular organization, tissue heterogeneity, and disease mechanisms in the urinary bladder. Such mapping is crucial for understanding cellular identity and the transcriptomic changes that occur during different stages of disease processes. With modern technology, one can follow spatial changes at an almost single-cell resolution, greatly upgrading our understanding of biological processes being studied. However, the starting point for all comparisons and analyses is healthy tissue in homeostasis. Since mouse models are mostly used for studying different urinary bladder disorders or treatments, it is vital to have spatial transcriptomic data for the mouse urinary bladder under basal, unchallenged conditions. Our analysis shows that the spatial transcriptomics bins display a gradient of gene expression, extending from the outer tissue layers toward the inner layers, rather than forming distinct, isolated domains. Cells originating from mesodermal progenitors likely undergo a gradual differentiation process, acquiring layer-specific features along the observed bin gradients. Similarly, urothelial cells, derived from a common endodermal progenitor, may follow a comparable transitional differentiation process[28].

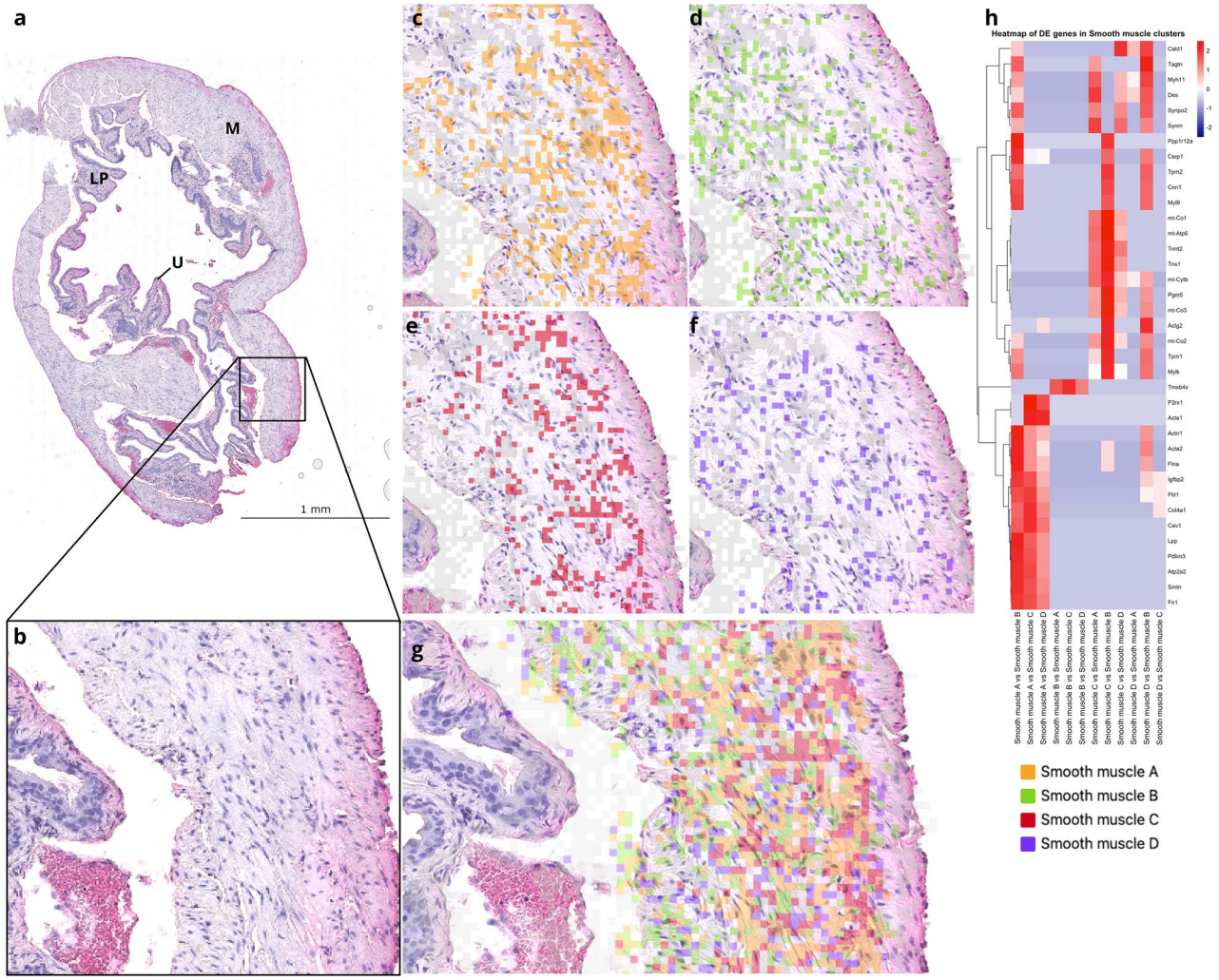

Fig. 6. High resolution spatial mapping and clustering of smooth muscle populations in the bladder using integrated transcriptomic annotation in Loupe Browser. (**a**) H&E-stained brightfield image of the entire bladder tissue section, highlighting the main layers: M - muscle, LP - lamina propria, and U - urothelium. (**b**) Magnified view of the central smooth muscle region shown in panel a. (**c**) Spatial clustering reveals a distinct smooth muscle A population (orange), identified within the bladder muscle layers. (**d**) Spatial clustering reveals a distinct smooth muscle B population (green), localized to specific regions within the muscle layers of the bladder. (**e**) Smooth muscle C population (red), visualized in its spatial context, demonstrating unique distribution patterns across the bladder muscle layer. (**f**) Smooth muscle D population (purple), displaying distinct clustering in the bladder muscle tissue. (**g**) Overlay visualization demonstrates the relative spatial organization of all smooth muscle clusters (A, B, C, D) across the bladder muscle layers, with the combined data highlighting the distinct and overlapping regions of each cluster within the bladder's muscle tissue. (**h**) Heatmap representing differentially expressed genes between the smooth muscle clusters (pairwise comparison).

The cluster annotation was approached both computationally and manually. Manual annotation was based on literature review, particularly Tabula Muris[27] and Mouse Cell Atlas (MCA)[23]. The results of manual annotation were tested and confirmed by computational annotation using the Seurat function AddModuleScore. The strength of spatial transcriptomics analysis arises from the preservation of spatial information of gene expression[4]. Rather than simply following existing literature annotations, we assigned more precise, histologically and spatially related names to our clusters. The Mouse Cell Atlas bladder single-cell RNAseq data identified 16 clusters, which can be broadly categorized as 3 stromal clusters, 5 epithelial clusters, 1 smooth muscle cluster, 4 immune cell clusters, and 3 vascular clusters[24]. In comparison, our dataset revealed 5 stromal clusters, 4 epithelial clusters, and 4 smooth muscle clusters with two of these stromal clusters associated with immune functions, namely the *Apoe* and *Cd74* stromal clusters. These discrepancies are probably the result of the chosen methodology protocols – scRNAseq relies on isolating individual cells, lysing them to release RNA, reverse transcribing to cDNA to prepare a cDNA library, which is then sequenced[16]. The crucial step is cell sorting to isolate individual cells, which relies on the known markers to separate the tissue into individual cells[16,17]. However, this approach

may overlook some cell subgroups that have yet to be discovered. On the other hand, spatial transcriptomics are based on chip-to-slide poly-T hybridization. Chip is spatially barcoded, and all the hybridized RNA from tissue is reverse transcribed and then sequenced[16,29]. In our analysis, we used the Seurat function FindNeighbours, which clusters all the cells with statistically similar expression patterns. Despite the different approaches, our spatial results mostly align with those in the Mouse Cell Atlas, especially considering the epithelial and stromal clusters. As expected, immune cell-related clusters showing *Cd74* (Log_2 fold change = 5.02, adjusted p-value = 0) and *Apoe* (Log_2 fold change = 6.66, adjusted p-value = 0) marked as top genes differ significantly from the rest of the urinary bladder clusters. Their uniqueness from the rest of the clusters is well observed in the UMAP representation (Fig. 2b).

Considering urothelial clusters, we obtained 4 of them while Mouse Cell Atlas lists 5. Our annotation overlaps when it comes to the umbrella and basal cells[24]. Since literature provides relatively thorough insight into these cells' markers, it was easy to identify particular clusters[3,8]. However, the process becomes interesting when we attempt to annotate two additional urothelial clusters. The separating layer between umbrella and basal cells is the intermediate cell layer, which is a monolayer in murine tissue compared with several layers in human bladder[3,6,11]. Histological position of the intermediate cell layer and the fact that gene expression of most genes is usually gradual along the tissue layers[30] indicate that intermediate cell markers will probably be the combination of both umbrella cell and basal cell markers, while at the same time not expressing all of their marker genes. This observation was consistent within our dataset, where we saw the apparent epithelial cluster with both basal and umbrella cell markers, such as uroplakin and *Krt5*, combined with a clearly much lower expression rate (Fig. 1d, S1). It is important to consider that different mouse strains or developmental stages may exhibit slight variations in urothelial stratification. By utilizing the spatial dimension of our approach, we were able to distinctly see the localization of such a cluster right between the umbrella and basal cell cluster layers. At the same time, we are aware that observed gene expression patterns in the intermediate urothelial cell layer, which appear to combine umbrella and basal cell markers, may be influenced by the lack of cell shape-based segmentation, leading to bins spanning multiple cell types and complicating the analysis. The last epithelial cluster to annotate evoked the biggest interest since it had some distinct umbrella cell features, yet it was stratified in a separate cluster (Fig. 4d). The cluster shows an expression pattern similar to the umbrella cells cluster expression pattern (Fig. 2b), except for several transcripts being expressed uniquely in the umbrella cell layer (Supplementary tables S1 and S3). Since the histological division of umbrella cells does not exist, nor is it morphologically visible, we hypothesize that umbrella cells show polarized gene expression – different mRNAs are located at the apical part of the cell. Although the elongated, flattened shape of umbrella cells does not inherently suggest polarity, considering the demanding environment these cells endure within the urinary bladder, the presence of such polarity is plausible and expected[6]. Furthermore, apical-basal polarity is essential for most epithelial cell functions[31]. Such stratification should be interpreted with caution, as it may reflect analytical rather than biological differences. In particular, the selection of parameters in the Seurat pipeline- such as the number of principal components used for dimensionality reduction and the resolution set during clustering – can strongly influence how cells are partitioned. These parameters may therefore lead to an artificial subdivision of umbrella cells that are otherwise transcriptionally similar. At the same time, we cannot rule out that the observed separation reflects genuine biological variation, such as polarized gene expression along the apical-basal axis of umbrella cells or microenvironmental influences specific to the superficial urothelium. Further experimental validation will be necessary to determine whether the stratification represents a true biological feature or an artifact of clustering. Both clusters share key umbrella cell markers, including *Sprr1a* as the top gene and uroplakins among top-expressed genes (Supplementary tables S1 and S2)[2,3] with the superficial urothelium cluster showing lower expression and fold changes compared to the umbrella cell cluster. Furthermore, cytokeratin 20 (*Krt20*) is known and widely accepted as the marker of umbrella cells[2,5,32]. It was used in the AddModuleScore function to help us conclude which of the four urothelial clusters most likely represent umbrella cells (S4). However, when analyzing the results of FindAllMarkers function for the cluster of Urothelium - Umbrella cells, *Krt20* is not found in the top 10 markers. Moreover, with Log_2 Fold Change of 4.13, *Krt20* is expressed in only 13.9% of the cells in the cluster (pct.1 = 0.139, S1). The importance of this marker probably lies in the fact that, alongside the long history of clinical use[5,32], no other cell type in the urinary bladder, besides the umbrella cells, expresses *Krt20*[2]. Our dataset shows several potential markers specific to umbrella cells with Log_2 Fold Change > 4 , and also expressed in a high percentage of these cells. Those markers are *Psca*, *Sprr2a3*, *Acer2*, *Snx31*, *Fabp4*, and *Fam25c* (Supplementary Table S2 and S3). It would be of high scientific as well as clinical value to further investigate the role and the expression pattern of these markers in pathological states of the urinary bladder.

Several stromal-enriched markers identified in our analysis highlight key processes involved in maintaining normal bladder tissue structure and function. Apolipoprotein E (*Apoe*), a lipid transport protein involved in cholesterol metabolism, cell signalling, and immune regulation, has been proposed as a potential bladder tissue biomarker[33,34]. *Cd74*, the invariant chain of MHC class II pathway, is broadly expressed in immune and stromal cells and plays roles in antigen presentation, immune modulation, and tissue remodelling; recent evidence also links it to regulatory T cell accumulation and function in tumors[35]. Matrix Gla Protein (*Mgp*), a vitamin K–dependent inhibitor of calcification expressed in smooth muscle and the ECM, has been implicated in cancer stem-like traits and tumor initiation, particularly in ovarian cancer, where its expression correlates with poor prognosis[36]. Decorin (*Dcn*), a structural proteoglycan critical for ECM organization and collagen fibrillogenesis in the bladder stroma, is notably downregulated in cancer-associated fibroblasts (CAFs), a shift that facilitates their pro-tumorigenic activation and promotes invasion and matrix remodelling[37,38]. These markers, while implicated in disease when dysregulated, reflect critical components of healthy bladder stroma in our reference dataset.

When inspecting smooth muscle clusters, there is a noticeable difference in our 4 clusters compared to only one cluster in the MCA single cell RNA seq analysis results[24]. This discrepancy could be due to methodology;

depending on the cell isolation method and cell sorting before sequencing, certain cells could be lost in the process[39]. Thanks to the spatial localization of the clusters, we can observe how different smooth muscle clusters intertwine (Figs. 3f and 6g), but at the same time show slightly different expression patterns. Notably, pairwise differential expression analysis revealed a consistent upregulation of Fn1, a well-established fibroblast and myofibroblast-associated gene[14,15], in the Smooth Muscle A cluster compared with clusters B–D (Fig. 6h, Supplementary Table S3), supporting the interpretation that this cluster exhibits a myofibroblast-like transcriptional signature, in line with previous single-cell RNA sequencing studies of the bladder that reported overlapping smooth muscle–fibroblast phenotypes rather than sharply distinct populations[40]. Spatial distribution of smooth muscle clusters (Fig. 3e) indicates that differences in gene expression are probably influenced by the cell microenvironment. As a result, the distinct segregation among clusters is visible from the lamina propria across the detrusor muscle layer, further out to the serous membrane. In consideration of Smooth muscle B cluster, it is observable that *Acta2* and *Actg2* rank as the top expressed genes (Fig. 1d, Supplementary Table S2). However, after the pairwise analysis (Fig. 6h, Supplementary table S3) comparing expression levels to other smooth muscle clusters, observed expression is not significantly different. *Synpo2* and *Synm*, with their activity in the formation of intermediate filaments[41,42] indicate the structural support role of the Smooth muscle C cluster, which differentially expresses these two genes.

The Smooth Muscle D cluster is the only cluster among the four that expresses collagen type I. While collagen type I is classically associated with the adventitia of blood vessels[43], its presence surrounding smooth muscle cells in the urinary bladder has been well described. Each bladder smooth muscle cell is embedded within an endomysial collagen network, and smooth muscle cells forming the detrusor are organized into bundles separated by collagen-rich connective tissue, often referred to as epimysium, although terminology may vary[44,45]. Histological analyses have demonstrated pronounced collagen staining surrounding smooth muscle bundles, providing structural support and contributing to coordinated contraction and innervation of detrusor muscle units[44].

In line with these observations, we propose that the Smooth Muscle D cluster represents a population of smooth muscle cells involved in the production of connective tissue enveloping smooth muscle bundles rather than vascular smooth muscle cells. This interpretation is further supported by the absence of significant expression of established vascular smooth muscle markers, including *Rgs5*, *Kcnj1*, and *Wtip*, in our dataset. Collectively, these findings are consistent with the known structural organization of bladder smooth muscle and underscore the functional heterogeneity of smooth muscle cells in tissue architecture, contraction, and extracellular matrix production.

For comparative purposes and to get the most out of spatial data obtained, we evaluated cluster delineation using both the standard FindNeighbors-based pipeline and the BANKSY[46] approach (Figs. 7S and 8S, 9S); however, immune-like stromal populations (*Apoe*$^+$ and *Cd74*$^+$ clusters) were not robustly preserved with BANKSY, and we therefore selected the FindNeighbors-based pipeline as it better captured the expected biological variability present in the tissue.

A comprehensive summary of identified cell type-specific and cluster-specific marker genes in bladder tissue, organized by tissue layer and ordered by descending $\log_2$ fold change within statistically filtered thresholds, is shown in Table 2. This annotated structure facilitates quick identification of dominant and highly specific marker genes relevant to cell type classification in spatial transcriptomics studies of the bladder. Additional marker gene information and data supporting these findings are provided in Supplementary Table S1.

These spatial transcriptomics results highlight top candidate markers with strong expression specificity in distinct bladder cell types and clusters. While interpreting such data remains complex, the highest-ranked markers represent promising targets for further functional validation. While spatial transcriptomics offers a resolution approaching single-cell level, 2 µm resolution could provide insights into subcellular expression differences, though with limitations such as lower nCounts and nFeatures. This higher resolution can reveal fine-grained details of gene expression but also presents challenges in terms of annotation accuracy and data sparsity. While publicly available single-cell RNA sequencing datasets such as the Mouse Cell Atlas (MCA)[24] and Tabula Muris[27] are invaluable for clustering and identifying cell types, they can sometimes miss or underrepresent certain cell populations due to challenges in tissue processing or isolation. In contrast, spatial transcriptomics offers a unique advantage by preserving the tissue architecture and enabling the analysis of cell types that are difficult to isolate separately for single-cell analysis. This method allows for the identification of these elusive cell types in situ, providing a more comprehensive and contextually accurate view of gene expression within the tissue. Overall, spatial transcriptomics provides unparalleled insight into tissue complexity in situ, and this study demonstrates its power to uncover previously unrecognized cellular heterogeneity and spatial gene expression patterns in the healthy urinary bladder.

Methods

Ethical statement

All mice were maintained under specific-pathogen-free (SPF) conditions at the Animal Facility of the University of Split (HR-POK-019), housed under a 12-hour light/dark cycle at an ambient temperature of 22 °C, with food and water provided *ad libitum*. Euthanasia was performed by cervical dislocation when the animals were 6–8 weeks of age. Several wild-type (WT) mice were euthanized under identical conditions as part of parallel experimental procedures; however, only one mouse (body weight 20.9 g, bladder weight 18.6 mg at the time of euthanasia) was used for the spatial transcriptomics analysis described in this study. All animals were routinely monitored for signs of distress and for all health parameters required by the facility. The study was approved by the Animal Welfare Committee of the University of Split and by the Ministry of Agriculture of the Republic of Croatia, Veterinary and Food Safety Directorate (approval number 525 – 10/0255-14-4). All procedures were conducted in full compliance with institutional and national guidelines, as well as the ARRIVE guidelines.

Bladder tissue layer	Cell type / cluster	Markers
Urothelium	Superficial cells	Upk1a, **Fmo5**, Upk2, Upk3a, **Sprr1a**, Upk1b, Uchl1, Sprr2a3, Krt18, Ivl, Krt8, **Gstm1**, Psca, Akr1b3, Krt7, Gsta4
	Umbrella cells	Fabp4, Fam25c, Psca, Sprr2a3, Acer2, Krt20, Upk2, Uchl1, S100a1, Clu, **Sprr1a**, Krt8, Snx31, **Upk3a**, Upk1b, **Upk1a**
	Intermediate cells	**Apoe**, Krt5, Gsta4, Krt19, **Gstm1**, Fmo5, Sprr1a, **Tmsb4x**
	Basal cells	Krt5, **Krt19**, Gsta4, Krt7, Akr1b3, **Gstm1**, Fmo5, Upk3a, Upk1b, Upk1a, S100a6, Sprr1a, **Tmsb4x**
Stromal cells (including lamina propria)	Fibroblasts (Col1a1+)	**Col1a1**, **Col1a2**, **Col3a1**
	Apoe+	**Apoe**
	Cd74+	**Cd74**, H2-Eb1
	Mgp+	**Mgp**
	Dcn+	**Dcn**
Smooth muscle	Smooth muscle A	Flna, Csrp1, Igfbp2, Myl9, Mylk, **Tpm2**, Tpm1, **Tagln**, **Myh11**, Des
	Smooth muscle B	**Tagln**, **Acta2**, Tpm1, Tpm2, **Myh11**, Actg2, Des, Cnn1, Mylk
	Smooth muscle C	Synm, Synpo2, **Des**, **Myh11**, Tpm1, Mylk, **Tagln**, Tpm2, Cnn1, Myl9
	Smooth muscle D	Col1a1, Des, Mylk, **Myh11**, **Tagln**, Tpm1, Cnn1, Cald1, **Tpm2**, Myl9

Table 2. Urinary bladder cell type markers.
Summary of Cell Type- and Cluster-Specific Marker Genes in Bladder Tissue Identified by Spatial Transcriptomics, Ranked by Log_2 Fold Change and Cell Expression Proportion. Genes and markers are listed for each cell type or cluster from the largest to the lowest log_2 fold change, filtered by significance thresholds for log_2 Fold Change and the percentage of expressing cells (pct.1). Font size and bolding correspond to the percentage of cells expressing a marker: the largest bold font denotes the highest pct.1 within the cluster, medium bold font indicates the second highest, and the smallest bold font signifies the third-highest pct.1—thus visually ranking marker prevalence per cluster. Marker color encodes specificity: red markers are unique to a single cluster, blue markers are present in two clusters, and green markers are expressed in all but one cluster across the tissue layer.

Collection and preparation of bladder samples

Male C57BL/6 mice (Jackson Laboratory) were euthanized at 6–8 weeks of age, and bladders were collected. Each bladder was bisected sagittally: one half was processed for formalin-fixed paraffin-embedded (FFPE) tissue block preparation while the other half was snap-frozen in liquid nitrogen and stored at − 80 °C (for possible further analyses). Tissues were fixed in 4% neutral buffered formalin (NBF), and processing was carried out according to the small tissue protocol[32]. Sections of 5 µm thickness were mounted on Superfrost™ Plus microscope slides (Fisherbrand™), deparaffinized, and stained with hematoxylin and eosin (H&E). Histological features were annotated by experienced pathologists to guide spatial transcriptomic analysis. Slides were imaged with a whole-slide scanner (Aperio AT2, Leica) at 20× magnification, then decoverslipped and decrosslinked according to standard guidelines (CG000684). Subsequent processing and library preparation followed the

Visium Spatial Gene Expression HD for FFPE protocol (CG000685). Briefly, tissue sections underwent probe hybridization, followed by enzymatic digestion with RNase and a tissue removal enzyme to release the probes, which were captured by the barcoded oligonucleotides on the Visium CytAssist slide. Probes were then extended, eluted, and transferred into new tubes for the library.

Total RNA extraction

Total RNA was extracted from formalin-fixed paraffin-embedded (FFPE) tissue sections, consecutive to those used for spatial transcriptomics, to assess RNA quality prior to the Visium HD 10x Genomics assay. Approximately 3–6 sections of 5–10 μm thickness were used per extraction and DV200. RNA purification was performed using a silica membrane-based spin column kit designed for FFPE samples (Qiagen RNeasy FFPE Kit), including DNase treatment to remove genomic DNA contamination, following manufacturer's instructions. RNA quantity and integrity were assessed by capillary electrophoresis (Agilent 4200 TapeStation). Samples with a DV200 value (percentage of RNA fragments longer than 200 base pairs) greater than 30% were considered suitable for downstream analysis.

Permeabilization, cDNA synthesis, tissue removal, probe release

Following staining, tissue sections underwent enzymatic permeabilization to enable mRNA capture by spatially barcoded probes on the Visium slide. Reverse transcription was performed in situ to synthesize cDNA from captured transcripts. The tissue was then removed, and the spatially barcoded cDNA was released for downstream processing.

HT sequencing

Before library loading, a quality check was performed on the HS-DNA chip using the TapeStation 4100 (Agilent). Samples were then diluted and loaded onto a NovaSeq 6000.

system (Illumina, San Diego, CA). Sequencing was carried out according to the manufacturer's instructions in paired-end mode (43/10/10/50 nt), targeting approximately 250 million clusters per sample. The number of clusters was calculated based on tissue occupancy of the total capture area (6.5 × 6.5 mm). Demultiplexing was performed using the bcl2fastq software (v2.20.0.422, Illumina).

cDNA library preparation and sequencing

Spatially barcoded cDNA libraries were prepared following the Visium HD Spatial Gene Expression Reagents Kits User Guide (CG000685). Brightfield H&E images and CytAssist images were aligned with the spatial capture areas using the Space Ranger pipeline (v3.1.3, 10x Genomics Cloud Analysis platform). Pre-built *Mus musculus* GRCm39 was used as reference genome for Space Ranger. Spot detection and visualization were performed to ensure accurate mapping of transcriptomic data to tissue morphology. For preliminary orientation and quality assessment, the .cloupe output file was examined in the Loupe browser.

Spot visualization and image alignment. Mapping, gene counting and demultiplexing

Raw FASTAQ sequences, alongside CytAssist image and brightfield H&E image were processed via Space Ranger v3.1.3 pipeline incorporated into 10x Genomics Cloud Analysis platform. Space Ranger performed alignment to the reference genome, gene counting, and demultiplexing of spatial barcodes. This step generated gene expression matrices mapped to spatial coordinates.

For preliminary orientation analysis .cloupe output file was used inside the Loupe browser.

Computational analysis

Comprehensive bioinformatic and biostatistical analyses of Space Ranger outputs were conducted using the Seurat package in R Studio version 4.5.0[25]. Data visualization and figure generation were performed with ggplot2[47]. All computational workflows were designed to ensure reproducibility and robustness of downstream analyses. Since data originated from a single tissue section, data merging or sketch-based subsampling techniques were not employed. All analyses were performed on spatial transcriptomic data binned at 8 μm × 8 μm resolution, balancing spatial precision and transcript detection sensitivity.

Quality control, dimensionality reduction and clustering

Quality control filtering excluded bins with mitochondrial RNA content exceeding 10% and bins with fewer than 40 unique molecular identifier (UMI) counts to ensure robust transcriptomic profiles. Gene expression data were then normalized and variance-stabilized using the SCTransform function implemented in Seurat. Dimensionality reduction was conducted via principal component analysis (PCA) retaining first 8 principal components for downstream clustering. Graph-based clustering employed FindNeighbors and FindClusters functions in Seurat with a resolution parameter set to 0.8. Differential expression analysis was performed using Seurat's default Wilcoxon rank-sum test. P-values were subsequently adjusted for multiple testing using the Bonferroni correction.

Visualization and spatial annotation of clusters

Clusters were visualized using Uniform Manifold Approximation and Projection (UMAP) and overlaid onto high-resolution tissue images. Spatial annotation of clusters was performed by integrating histological features and reference datasets and reference datasets such as the Mouse Cell Atlas[24] and Tabula Muris[27] to assign putative cell type identities.

Differential gene expression analysis (DGEA) and expression programs

Clusters were manually annotated based on an extensive literature review[2,6,11,14–16] and by referencing established datasets such as the Mouse Cell Atlas[24] and Tabula Muris[27]. To validate our annotations, we applied the Seurat function AddModuleScore, which calculates the relative expression of predefined marker gene sets, thereby confirming cluster identities through quantitative enrichment analysis.

Nucleus segmentation

Nuclei were segmented from high-resolution histological images using a StarDist-based deep learning workflow implemented in Jupyter notebooks. A pretrained 2D StarDist model was applied to detect star-convex nuclear objects, and segmentation masks were converted into labeled nuclei. Centroid coordinates (x, y) were extracted for each nucleus.

Gene expression counts were aggregated at the nucleus level, generating a gene-by-nucleus count matrix and a corresponding spatial coordinate table. Nuclei with zero detected transcripts were excluded prior to downstream analysis, resulting in filtered count and coordinate matrices for spatial clustering.

BANKSY spatial clustering

Nucleus-level count data were imported into R and converted into a 'SpatialExperiment' object (SpatialExperiment v1.14.0, SummarizedExperiment v1.34.0, SingleCellExperiment v1.26.0). Library size normalization was performed using `computeLibraryFactors` from scuttle v1.14.0, and normalized counts were generated using `normalizeCounts`. Matrix operations were handled using Matrix v1.7.4.

Spatially informed clustering was performed using Banksy v1.0.0. Spatial smoothing was computed with `computeBanksy()` using a geometric neighbourhood size of $k = 25$ and spatial weighting parameter $\alpha = 0.15$. Dimensionality reduction was performed with `runBanksyPCA()` (40 principal components), followed by clustering using `clusterBanksy()` (resolution = 0.55) and visualization with `runBanksyUMAP()`. Cluster-specific marker genes were identified using `scran v1.32.0`. Visualization and plotting were performed using ggplot2 v4.0.2, and data manipulation was conducted with dplyr v1.2.0.

Limitations of the study

Due to financial constraints, this study was unable to include biological replicates, which would have enhanced the statistical robustness of the findings. While this limitation is acknowledged, we believe the study still provides valuable insights into spatial transcriptomics, particularly for urinary bladder tissue, and offers a comprehensive review of known and potential biomarkers in this field.

The QC plots (Supplementary figures S1-S3) show lower modes for nFeatures and nCounts than typically expected for high-quality 8 µm bin data. While we cannot definitively determine whether RNA degradation occurred during processing, we emphasize that it likely contributed to reduced sensitivity in downstream analyses.

Figures 4 and 5 show some misalignment with H&E-stained tissue, likely due to tissue shift during processing. The sectioning, expansion in the bath, and shipping conditions may have contributed to slight displacement of tissue layers, particularly the urothelium and lamina propria. While this misalignment did not affect the overall findings, it did impact the visual alignment of spatial bins with the H&E staining image.

Data availability

The datasets generated and/or analyzed during the current study are available in the ArrayExpress repository [[https://www.ebi.ac.uk/biostudies/ArrayExpress/studies/E-MTAB-15675?key=4b45349a-dc62-4bdc-912a-6a4bf3781602](https:/www.ebi.ac.uk/biostudies/ArrayExpress/studies/E-MTAB-15675?key=4b45349a-dc62-4bdc-912a-6a4bf3781602) and ACCESSION NUMBER TO DATASETS: E-MTAB-15675 (8 × 8 µm bins) and E-MTAB-16522 (2 × 2 µm bins)].The code for R script with Seurat pipeline for Spatial Transcriptomics analysis alongside all the package versions used in this manuscript is available at GitHub ([https://github.com/agelemanovic/ST_mouse_bladder](https:/github.com/agelemanovic/ST_mouse_bladder)).

Code Availability

The code for R script with Seurat pipeline for Spatial Transcriptomics analysis alongside all the package versions used in this manuscript is available at GitHub (https://github.com/agelemanovic/ST_mouse_bladder).

Received: 3 October 2025; Accepted: 28 February 2026
Published online: 16 March 2026

References

1. Su, X., Tao, Y., Chen, F., Han, X. & Xue, L. Trends in the global, regional, and national burden of bladder cancer from 1990 to 2021: an observational study from the global burden of disease study 2021. *Sci. Rep.* **15**, 1–19. https://doi.org/10.1038/s41598-025-92033-5 (2025).
2. Jafari, N. V. & Rohn, J. L. The urothelium: a multi-faceted barrier against a harsh environment. *Mucosal Immunol.* **15**, 1127–1142. https://doi.org/10.1038/S41385-022-00565-0 (2022).
3. Khandelwal, P., Abraham, S. N. & Apodaca, G. Cell biology and physiology of the uroepithelium. *Am. J. Physiol. Ren. Physiol.* 297. https://doi.org/10.1152/AJPRENAL.00327.2009 (2009).
4. Hallou, A., He, R., Simons, B. D. & Dumitrascu, B. A computational pipeline for spatial mechano-transcriptomics. *Nat. Methods.* **22**, 737–750. https://doi.org/10.1038/s41592-025-02618-1 (2025).
5. Sanguedolce, F. et al. Diagnostic and prognostic roles of CK20 in the pathology of urothelial lesions. A systematic review. *Pathol. Res. Pract.* **215**, 152413. https://doi.org/10.1016/J.PRP.2019.04.005 (2019).

6. Dalghi, M. G., Montalbetti, N., Carattino, M. D. & Apodaca, G. The urothelium: Life in a liquid environment. *Physiol. Rev.* **100**, 1621–1705. https://doi.org/10.1152/PHYSREV.00041.2019 (2020).
7. Andersson, K. E. & Arner, A. Urinary bladder contraction and relaxation: Physiology and pathophysiology. *Physiol. Rev.* **84**, 935–986. https://doi.org/10.1152/PHYSREV.00038.2003 (2004).
8. Birder, L. A. & de Groat, W. C. Mechanisms of Disease: involvement of the urothelium in bladder dysfunction. *Nat. Clin. Pract. Urol.* **4**, 46. https://doi.org/10.1038/NCPURO0672 (2007).
9. Bunduki, G. K. et al. Virulence factors and antimicrobial resistance of uropathogenic *Escherichia coli* (UPEC) isolated from urinary tract infections: a systematic review and meta-analysis. *BMC Infect Dis.* **21**, 1–13. https://doi.org/10.1186/S12879-021-06435-7 (2021).
10. Park, J. H. et al. Statin prevents cancer development in chronic inflammation by blocking interleukin 33 expression. *Nat. Commun.* **15**, 1–15. https://doi.org/10.1038/s41467-024-48441-8 (2024).
11. Deltourbe, L. G., Durand, M., Costas, A. & Ingersoll, M. A. A bladder blueprint to build better models for understanding homeostasis and disease. *Nat. Rev. Urol.* 1–13. https://doi.org/10.1038/s41585-025-01013-x (2025).
12. Andersson, K. E. & McCloskey, K. D. Lamina propria: The functional center of the bladder? *Neurourol. Urodyn.* **33**, 9–16. https://doi.org/10.1002/NAU.22465 (2014).
13. Muhl, L. et al. Single-cell analysis uncovers fibroblast heterogeneity and criteria for fibroblast and mural cell identification and discrimination. *Nat. Commun.* **11**, 1–18. https://doi.org/10.1038/s41467-020-17740-1 (2020).
14. Clayton, D. R. et al. Studies of ultrastructure, gene expression, and marker analysis reveal that mouse bladder PDGFRA1 interstitial cells are fibroblasts. *Am. J. Physiol. Ren. Physiol.* **323**, F299–321. https://doi.org/10.1152/AJPRENAL.00135.2022 (2022).
15. Apodaca, G. Defining the molecular fingerprint of bladder and kidney fibroblasts. *Am. J. Physiol. Ren. Physiol.* **325**, F836–F856. https://doi.org/10.1152/AJPRENAL.00284.2023 (2023).
16. Baker, D. et al. A Cellular Reference Resource for the Mouse Urinary Bladder. *bioRxiv* https://doi.org/10.1101/2021.09.20.461121 (2021). 2021.09.20.461121.
17. Yu, Z. et al. Single-cell transcriptomic map of the human and mouse bladders. *J. Am. Soc. Nephrol.* **30**, 2159–2176. https://doi.org/10.1681/ASN.2019040335 (2019).
18. Younesi, F. S., Miller, A. E., Barker, T. H., Rossi, F. M. V. & Hinz, B. Fibroblast and myofibroblast activation in normal tissue repair and fibrosis. *Nat. Rev. Mol. Cell. Biol.* **25**, 617–638. https://doi.org/10.1038/s41580-024-00716-0 (2024).
19. Buechler, M. B. et al. Cross-tissue organization of the fibroblast lineage. *Nature* **593**, 575–579. https://doi.org/10.1038/S41586-021-03549-5 (2021).
20. Bowyer, G. S., Loudon, K. W., Suchanek, O. & Clatworthy, M. R. Tissue Immunity in the Bladder. *Annu. Rev. Immunol.* **40**, 499–523. https://doi.org/10.1146/annurev-immunol-101220-032117 (2022).
21. Jaslove, J. M. & Nelson, C. M. Smooth muscle: a stiff sculptor of epithelial shapes. *Philosophical Trans. Royal Soc. B: BiologicaSciences.* **373**, 20170318. https://doi.org/10.1098/RSTB.2017.0318 (2018).
22. Tasian, G., Cunha, G., Baskin, L., Frank, F. & Urological, H. Smooth Muscle Differentiation and Patterning in the Urinary Bladder. *Differentiation* **80**, 106. https://doi.org/10.1016/J.DIFF.2010.05.004 (2010).
23. Sam, P., Nassereddin, A., LaGrange, C. A. & Anatomy Abdomen and Pelvis: Bladder Detrusor Muscle. *StatPearls* (StatPearls Publishing, 2023).
24. Han, X. et al. Mapping the Mouse Cell Atlas by Microwell-Seq. *Cell* **172**, 1091–1107e17. https://doi.org/10.1016/J.CELL.2018.02.001 (2018).
25. Hao, Y. et al. Dictionary learning for integrative, multimodal and scalable single-cell analysis. *Nat. Biotechnol.* **42**, 293–304. https://doi.org/10.1038/S41587-023-01767-Y (2024).
26. Becht, E. et al. Dimensionality reduction for visualizing single-cell data using UMAP. *Nat. Biotechnol.* **37**, 38–44. https://doi.org/10.1038/nbt.4314 (2018).
27. Schaum, N. et al. Single-cell transcriptomics of 20 mouse organs creates a Tabula Muris. *Nature* **562**, 367–372. https://doi.org/10.1038/S41586-018-0590-4 (2018).
28. Jackson, A. R., Narla, S. T., Bates, C. M. & Becknell, B. Urothelial progenitors in development and repair. *Pediatr. Nephrol.* **37**, 1721. https://doi.org/10.1007/S00467-021-05239-W (2021).
29. Marx, V. Method of the Year: spatially resolved transcriptomics. *Nat. Methods*. **18**, 9–14. https://doi.org/10.1038/s41592-020-01033-y (2021).
30. Kueckelhaus, J. et al. Inferring histology-associated gene expression gradients in spatial transcriptomic studies. *Nat. Commun.* **15**, 1–19. https://doi.org/10.1038/s41467-024-50904-x (2024).
31. Buckley, C. E. & St Johnston, D. Apical–basal polarity and the control of epithelial form and function. *Nat. Rev. Mol. Cell. Biol.* **23**, 559–577. https://doi.org/10.1038/s41580-022-00465-y (2022).
32. Bejrananda, T., Kanjanapradit, K., Saetang, J. & Sangkhathat, S. Impact of immunohistochemistry-based subtyping of GATA3, CK20, CK5/6, and CK14 expression on survival after radical cystectomy for muscle-invasive bladder cancer. *Sci. Rep.* **11**, 21186. https://doi.org/10.1038/S41598-021-00628-5 (2021).
33. Huang, Y., Mahley, R. W. & Apolipoprotein, E. Structure and Function in Lipid Metabolism, Neurobiology, and Alzheimer's Diseases. *Neurobiol. Dis.* **72**, 3. https://doi.org/10.1016/J.NBD.2014.08.025 (2014).
34. Ghafouri-Fard, S., Nekoohesh, L. & Motevaseli, E. Bladder cancer biomarkers: review and update. *Asian Pac. J. Cancer Prev.* **15**, 2395–2403. https://doi.org/10.7314/APJCP.2014.15.6.2395 (2014).
35. Bonnin, E. et al. CD74 supports accumulation and function of regulatory T cells in tumors. *Nat. Commun.* **15**, 1–19. https://doi.org/10.1038/S41467-024-47981-3 (2024).
36. Nieddu, V. et al. Matrix Gla Protein drives stemness and tumor initiation in ovarian cancer. *Cell. Death Dis.* **14**, 1–16. https://doi.org/10.1038/S41419-023-05760-W (2023).
37. Nicolas, A. M. et al. Inflammatory fibroblasts mediate resistance to neoadjuvant therapy in rectal cancer. *Cancer Cell.* **40**, 168–184e13. https://doi.org/10.1016/j.ccell.2022.01.004 (2022).
38. Neill, T., Schaefer, L., Iozzo, R. V. & Decorin A Guardian from the Matrix. *Am. J. Pathol.* **181**, 380. https://doi.org/10.1016/J.AJPATH.2012.04.029 (2012).
39. Jovic, D. et al. Single-cell RNA sequencing technologies and applications: A brief overview. *Clin. Transl Med.* **12**, 694. https://doi.org/10.1002/CTM2.694 (2022).
40. Cañizo, C. G. et al. Characterisation of the tumour microenvironment and PD-L1 granularity reveals the prognostic value of cancer-associated myofibroblasts in non-invasive bladder cancer. *Oncoimmunology* **14**, 2438291. https://doi.org/10.1080/2162402X.2024.2438291 (2024).
41. Paulin, D. et al. Synemin-related skeletal and cardiac myopathies: An overview of pathogenic variants. *Am. J. Physiol. Cell. Physiol.* **318**, 709–718. https://doi.org/10.1152/ajpcell.00485.2019 (2020).
42. Zheng, Z. & Song, Y. Synaptopodin-2: a potential tumor suppressor. *Cancer Cell.* **23**, 158. https://doi.org/10.1186/S12935-023-03013-6 (2023).
43. Ponticos, M., Partridge, T., Black, C. M., Abraham, D. J. & Bou-Gharios, G. Regulation of Collagen Type I in Vascular Smooth Muscle Cells by Competition between Nkx2.5 and δEF1/ZEB1. *Mol. Cell. Biol. Informa UK Ltd.* **24**, 6151. https://doi.org/10.1128/mcb.24.14.6151-6161.2004 (2004).
44. Borsdorf, M. et al. Locational and directional dependencies of smooth muscle properties in pig urinary bladder. *Front. Physiol.* **10**, 432698. https://doi.org/10.3389/FPHYS.2019.00063/BIBTEX (2019).

45. Deveaud, C. M. et al. Molecular analysis of collagens in bladder fibrosis. *J. Urol.* **160**, 1518–1527. https://doi.org/10.1016/S0022-5347(01)62606-5 (1998).
46. Singhal, V. et al. BANKSY unifies cell typing and tissue domain segmentation for scalable spatial omics data analysis. *Nat. Gen.* **56**, 431–441. https://doi.org/10.1038/s41588-024-01664-3 (2024).
47. Wickham, H. ggplot2 (Springer International Publishing, 2016). https://doi.org/10.1007/978-3-319-24277-4

Acknowledgements
This work was supported by the Croatian Science Foundation under grant numbers IP-2020-02-8921, DOKN-POO-2023-10-7217 and IP-UNIST-30.

Author contributions
The study was conceived and designed by NM and JT. Methodology development was carried out by NM, AG, KP and JT. Sample collection and gathering were performed by NM and BMR. Data acquisition was conducted by NM, DL, CO, and JKP. Data analysis and interpretation were performed by NM, AG, KP, KV, and JT. Visualization was done by NM and AG. Data interpretation, review, and editing were carried out by NM, KP, DL, CO, IMT, IN, JKP, and JT. Writing and review of the manuscript were done by NM, KP, and JT. Project administration, supervision, and oversight were provided by JT. Funding acquisition was handled by JT.

Funding
This work was supported by the Croatian Science Foundation under grant numbers IP-2020-02-8921, DOKN-POO-2023-10-7217 and IP-UNIST-30.

Declarations

Competing interests
The authors declare no competing interests.

Additional information
Supplementary Information The online version contains supplementary material available at https://doi.org/10.1038/s41598-026-42931-z.

Correspondence and requests for materials should be addressed to J.T.